

Soft Modes, Localization and Two-Level Systems in Spin Glasses

M. Baity-Jesi

*Departamento de Física Teórica I, Universidad Complutense, 28040 Madrid, Spain,
Dipartimento di Fisica, La Sapienza Università di Roma, 00185 Roma, Italy, and
Instituto de Biocomputación y Física de Sistemas Complejos (BIFI), 50009 Zaragoza, Spain.*

V. Martín-Mayor

*Departamento de Física Teórica I, Universidad Complutense, 28040 Madrid, Spain, and
Instituto de Biocomputación y Física de Sistemas Complejos (BIFI), 50009 Zaragoza, Spain.*

G. Parisi

*Dipartimento di Fisica, NANOTEC-CNR, Soft and Living Matter Laboratory and INFN,
La Sapienza Università di Roma, 00185 Roma, Italy.*

S. Perez-Gaviro

*Centro Universitario de la Defensa, Carretera de Huesca s/n, 50090 Zaragoza, Spain, and
Instituto de Biocomputación y Física de Sistemas Complejos (BIFI), 50009 Zaragoza, Spain.*

(Dated: March 2, 2024)

In the three-dimensional Heisenberg spin glass in a random field we study the properties of the inherent structures that are obtained by an instantaneous cooling from infinite temperature. For not too large field the density of states $g(\omega)$ develops localized soft *plastic* modes and reaches zero as ω^4 (for large fields a gap appears). When we perturb the system adding a force along the softest mode one reaches very similar minima of the energy, separated by small barriers, that appear to be good candidates for classical two-level systems.

PACS numbers: 75.10.Nr, 75.40.Mg,

Keywords: Spin glass, inherent structure, density of states, two-level system, glass transition, localization, Heisenberg model, boson peak, soft modes

Supercooled liquids and amorphous solids exhibit an excess of low-energy excitations, compared with their crystalline counterparts [1], in which at low frequencies the density of states (DOS) $g(\omega)$ has a Debye behavior $g(\omega) \propto \omega^{d-1}$ in d spatial dimensions. This excess of low-frequency modes is called *Boson peak* [2, 3] and it is located at a small, but non zero frequency.

What happens at much lower frequency? Obviously we find phonons, but what is there beyond phonons? Were it possible to disregard Goldstone bosons, a scaling $g(\omega) \propto \omega^\delta$, with $\delta = 3$ or 4 has been suggested for disordered systems [4, 5]. Still, this has not been demonstrated nor observed. It has been stressed by [6–8] that there are localized plastic modes, whose spectral density reaches zero when ω goes to zero. These modes are subdominant in the small frequency region: They are called “*plastic*” because they dominate the plastic response. These extra small frequency modes may be related to the behaviour of hard spheres at jamming [9–13].

Replica theory offers an explanation for these extra modes. At low enough temperatures, strongly disordered mean field models undergo spontaneous full replica symmetry breaking (RSB). Full RSB implies a complex energy landscape with a hierarchical structure of states and a large amount of degenerate minima separated by small free energy barriers [14, 15]. As a consequence, zero-temperature equilibrium configurations can be deformed

at essentially no energy cost through easy-deformation patterns, that we name soft modes [13, 16]. These modes are localized in space, but non-exponentially. In fact, the zero temperature phase transition from the replica symmetric phase to the RSB phase is accompanied by a divergence of the localization length [17].

More often than not, finding low-lying energy minima of glassy systems is a NP problem [18]. Here we study the behavior of inherent structures (IS), local minima of the energy obtained by relaxing the system from high temperature (the thermal protocol should not change drastically the DOS, at least if we remain in the replica symmetric phase, see the appendix). In our study we need a model with continuous degrees of freedom. The Heisenberg model, where the spins are three-dimensional unitary vectors, is an epitome of the spin glass [19].

The global rotational-symmetry of the Heisenberg spin glass has far-reaching consequences. The corresponding symmetry in structural glasses is translation symmetry (which has similar implications). The Goldstone mechanism induces soft excitations in the form of spin waves [20]. Even in disordered systems, spin-waves are efficiently labelled by their wavevector, especially at low frequencies (see e.g. [21]). As a consequence, we have a Debye spectrum $g(\omega) \propto \omega^{d-1}$, i.e. extended spin waves (for structural glasses the situation is slightly more com-

plicated.¹ These symmetry-induced modes mask the physics we aim to investigate.

Thus, we add a random magnetic field (RF) to wipe out the symmetries. Indeed, mean field suggests that, if small enough, our RF does not destroy the glass phase [26]. In a RF, spin waves have a positive frequency, even for vanishing wavevector (e.g. a ferromagnet in a RF has no soft-modes). Therefore, the RF exposes the (possibly localized) plastic modes that interest us. The resulting spectrum has no reason to be Debye as it does not result from plain waves. Yet, a crossover to the Debye regime should appear when the RF is small. A similar procedure of symmetry removal has been carried through in glass-forming liquids, by pinning a certain fraction of particles [27–31]. The Heisenberg spin offers the advantage of allowing us to simulate unprecedentedly large systems, letting us observe scalings of several orders of magnitude.

Here, we study the ISs starting from initial random configurations and we do find that they are marginally stable states: the distribution of eigenvalues of the Hessian matrix stretches down to zero as a power law, and it is unrelated to symmetries in the system. Furthermore, we find that the soft modes are localized. We also take in account the anharmonic effects due to the complexity of the energy landscape. We find that the energy barriers along the softest mode are extremely small and that they connect very similar states with an strong relationship, that we propose as a operational definition of classical two-level systems (TLS) [32].

Model We study the three-dimensional Heisenberg spin glass in a RF. The dynamic variables are three-dimensional spins $\vec{s}_{\mathbf{x}}$, placed at the vertices \mathbf{x} of a cubic lattice of linear size L with unitary spacings. We have therefore $N = L^3$ spins, and $2N$ degrees of freedom (dof) due to the normalization constraint $\vec{s}_{\mathbf{x}}^2 = 1$. The Hamiltonian is

$$\mathcal{H}_{\text{RF}}(|\vec{s}\rangle) = - \sum_{|\mathbf{x}-\mathbf{y}|=1} J_{\mathbf{xy}} \vec{s}_{\mathbf{x}} \cdot \vec{s}_{\mathbf{y}} - \sum_{\mathbf{x}} \vec{h}_{\mathbf{x}} \cdot \vec{s}_{\mathbf{x}}, \quad (1)$$

where the fields $\vec{h}_{\mathbf{x}}$ are random vectors chosen uniformly from the sphere of radius H_{amp} , and $|\vec{s}\rangle$ indicates the full configuration of spins $\vec{s}_{\mathbf{x}}$. The RF breaks all rotational and translational symmetry, removing the Goldstone bosons. The couplings J_{ij} are fixed, Gaussian distributed, with $\overline{J_{\mathbf{xy}}} = 0$ and $\overline{J_{\mathbf{xy}}^2} = J^2$, where $\overline{(\dots)}$ is the average over the disorder.

We simulated on systems of linear lattice size $L = 12, 24, 48, 96, 192$. We chose always $J = 1$, and we compared it with $H_{\text{amp}} = 0.01, 0.05, 0.1, 0.5, 1, 5, 10, 50$. In

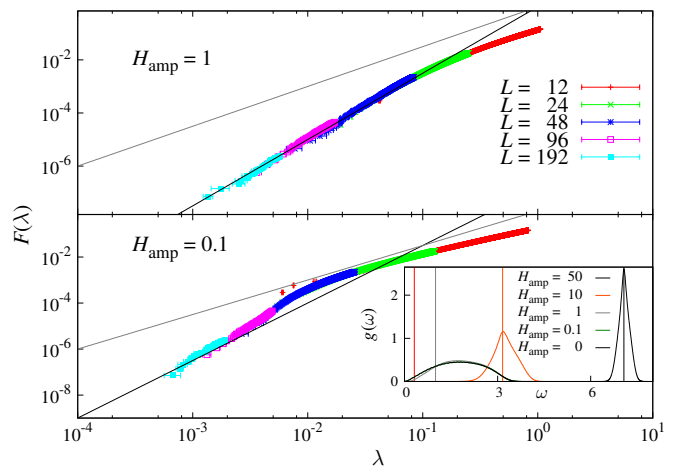


Figure 1. Cumulative $F(\lambda)$ of the spectrum of \mathcal{M} . In each plot we show black a reference curve representing the power law $\lambda^{2.5}$, and a grey line indicating the Debye behavior $\lambda^{1.5}$. *Inset*: The DOS $g(\omega)$ calculated with the method of the moments. In the limit of a diagonal hamiltonian ($J = 0$) the DOS would be a delta function centered on $\omega^2 = H_{\text{amp}}$. This value is represented with vertical lines.

the appendix we summarize the simulation parameters. The case $H_{\text{amp}} = 0$ will be treated in a future work [33], because it requires a different type of analysis, since the spin waves do not hybridize with the bulk of the spectrum.

Density of states We calculate the dynamical matrix as the Hessian matrix \mathcal{M} of Hamiltonian (1), calculated at the ISs. In the appendix we report how the ISs were obtained, we motivate the choice of the algorithm and the temperature of the starting configuration $|\vec{s}\rangle$ for the energy minimizations, and we show how the Hessian matrix \mathcal{M} was calculated.

Once \mathcal{M} is known, from each simulated H_{amp} we calculate the spectrum of the eigenvalues $\rho(\lambda)$ or equivalently, in analogy with plane waves [34], the DOS $g(\omega)$, by defining $\lambda = \omega^2$. We measure the DOS both with the method of the moments [35–37], and by explicitly computing with Arpack [38] the lowest eigenvalues.²

We find that, although for large fields there is a gap in the DOS when the field is small enough the gap disappears and the DOS goes to zero developing soft modes (Fig. 1, inset).

We focus on the $\rho(\lambda)$ for small λ , or even better on its cumulative function $F(\lambda) = \int_0^\lambda \rho(\lambda') d\lambda'$. If $F(\lambda)$ reaches zero as a power law, we can define three exponents δ, α

¹ In the case of structural glasses, the authors of [22–25] find $g(\omega) \sim \omega^2$ is valid for any spatial dimension. The origin of this different behaviour should be investigated carefully.

² The method of the moments returns the full density of states, but it is not precise at the tails. With Arpack we can calculate exactly the smallest eigenvalues, but only a small number of them. So, when we want to show the whole spectrum we need to use the method of the moments, while when we show the softest part of the spectrum we need Arpack.

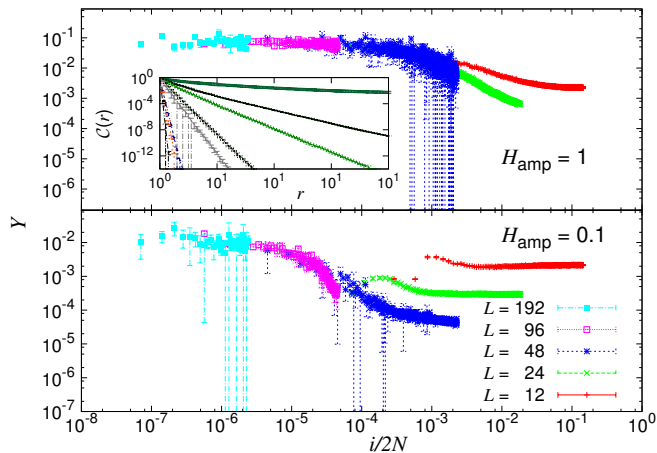


Figure 2. Inverse participation ratio as a function of the normalized rank $i/2N$ of the eigenvector ($i = 1$ has the smallest eigenvalue, $i = 2$ the second smallest, ...), for $H_{\text{amp}} = 1$ (top) and $H_{\text{amp}} = 0.1$ (bottom). **Inset:** Correlation function $\mathcal{C}(r)$ extracted from the eigenvectors, for fields (from top to bottom) $H_{\text{amp}} = 0.01, 0.05, 0.1, 0.5, 1, 5, 10, 50$ in $L = 192$ lattices. See the appendices for a close-up. For the smallest H_{amp} our data do not display an exponential decay, which could be caused by a localization length larger than the system size.

and γ , that describe how the functions g, ρ and F go to zero for small λ (or ω):

$$g(\omega) \sim \omega^\delta, \quad \rho(\lambda) \sim \lambda^\alpha, \quad F(\lambda) \sim \lambda^\gamma, \quad (2)$$

where the exponents are related by $\delta = 2\alpha + 1 = 2\gamma - 1$. In the absence of a field one expects a Debye-like behavior $\delta = d - 1 = 2$, $\alpha = 0.5$, $\gamma = 1.5$ [21].

In Fig. 1 we show the function $F(\lambda)$ for fields $H_{\text{amp}} = 0.1, 1$. The plots are compared with the Debye behavior $\lambda^{1.5}$ and with the power law behavior $\lambda^{2.5}$, because our data suggests a universal behavior around $\gamma = 2.5$ ($\delta = 4$, $\alpha = 1.5$) for all H_{amp} that does not exhibit a gap.³ See the appendix for the data on other H_{amp} .

When the field is small we remark a change of trend from $\gamma \approx 2.5$ to $\gamma < 1.5$ at a value λ^* . Very roughly speaking, the crossover point goes as $\lambda^* \sim H_{\text{amp}}^{-1}$, maybe indicating the presence of a boson peak.

Localization Similarly as it happens in other types of disordered systems [39–41], the soft modes are localized, meaning that the eigenvectors $|\vec{\pi}_n\rangle$ are dominated by few components. A nice localization probe is the inverse participation ratio $Y_n = \frac{\sum_{\mathbf{x}} (|\vec{\pi}_{n,\mathbf{x}}|^2)^2}{(\sum_{\mathbf{x}} |\vec{\pi}_{n,\mathbf{x}}|^2)^2}$. If the eigenvector $|\vec{\pi}_n\rangle$ is fully localized in one site, then $Y_n = 1$, whereas if it is fully delocalized, $Y_n = 1/N$. In Fig. 2 we show that the

softer the eigenvectors the more localized they are, and for infinitely large systems there is probably a localization threshold that separates a small fixed percentage of localized eigenvectors from the delocalized bulk ones.

The localization length increases as H_{amp} decreases, see Fig. 2–inset. In fact, a RSB transition should cause a localization transition at the critical H_{amp} [17]. However, it is unclear whether or not an RSB transition would leave a trace in infinite-temperature ISs.⁴

Anharmonicity We go beyond the harmonic approximation, and take in account the relationship between different ISs.

We study the reaction of the system to a force along a direction $|\pi\rangle$, normalized to one: $\sum_{\mathbf{x}} \vec{\pi}_{\mathbf{x}}^2 = 1$. We examine the softest mode, that is localized, and we compare it with the behavior of the eigenvectors in bulk of the $\rho(\lambda)$, that are delocalized. Therefore we choose $|\pi\rangle = |\pi_0\rangle$ (softest mode) and $|\pi\rangle = |\pi_{\text{RAND}}\rangle$, a vector whose components are chosen at random. The vector $|\pi_{\text{RAND}}\rangle$ is not an eigenvector of \mathcal{M} , but it is a random linear combination of all the eigenvectors of the system. Since the bulk eigenvectors overwhelm the soft modes by number, $|\pi_{\text{RAND}}\rangle$ will be representative of the bulk behavior.

With the application of a forcing along $|\vec{\pi}\rangle$, Hamiltonian (1) is modified in

$$\mathcal{H}_{\text{F}}(|\vec{s}\rangle) = - \sum_{\|\mathbf{x}-\mathbf{y}\|=1} J_{\mathbf{x}\mathbf{y}} \vec{s}_{\mathbf{x}} \cdot \vec{s}_{\mathbf{y}} - \sum_{\mathbf{x}} \left(\vec{h}_{\mathbf{x}} + A_{\text{F}} \vec{\pi}_{\mathbf{x}} \right) \cdot \vec{s}_{\mathbf{x}}, \quad (3)$$

where A_{F} is the amplitude of the forcing. If $A_{\text{F}} > 0$ ($A_{\text{F}} < 0$), spins tilt toward (against) $|\vec{\pi}\rangle$. We can measure quantitatively this response of the system to the forcing through $\hat{m} = \sum_{\mathbf{x}} \vec{s}_{\mathbf{x}} \cdot \vec{\pi}_{\mathbf{x}}$. We are interested in forcings A_{F} both in the linear response regime, and just out of it.

We stimulate the system with forcings of increasing amplitude, and study when this kicks the system out of the original inherent structure. Ideally, the forcing amplitude A_{F} would grow continuously. We simplify the analysis by choosing $A_{\text{F}} = \mathcal{A}i_h$, where \mathcal{A} is a carefully tuned amplitude (see below) while i_h is an integer. The unperturbed Hamiltonian corresponds to $i_h = 0$, while $i_h = \pm N_{\text{F}}$ is our maximum forcing (note that $\pm i_h$ forcings are not equivalent due to anharmonicities).

This is how we check if new states were encountered upon increasing the forcing: (i) For each i_h , start from the IS $|\vec{s}^{(\text{IS})}\rangle$ of the unperturbed Hamiltonian \mathcal{H}_{RF} . (ii) From $|\vec{s}^{(\text{IS})}\rangle$ minimize the energy using $\mathcal{H}_{\text{F}}(i_h)$, and find a new IS for the perturbed system, $|\text{IS}(i_h)\rangle$. (iii) From $|\text{IS}(i_h)\rangle$ minimize the energy again, using $\mathcal{H}_{\text{F}}(0) = \mathcal{H}_{\text{RF}}$, and find the IS $|\text{IS}^*\rangle$ (with elements $\vec{s}_{\mathbf{x}}^{(\text{IS}^*)}$). (iv) If

³ The value $\gamma = 2.5$ is also hypothesized in [4], through a fourth-order expansion of a single coordinate potential of the minimum of the energy.

⁴ Inherent structures that were obtained by relaxing an infinite-temperature configuration.

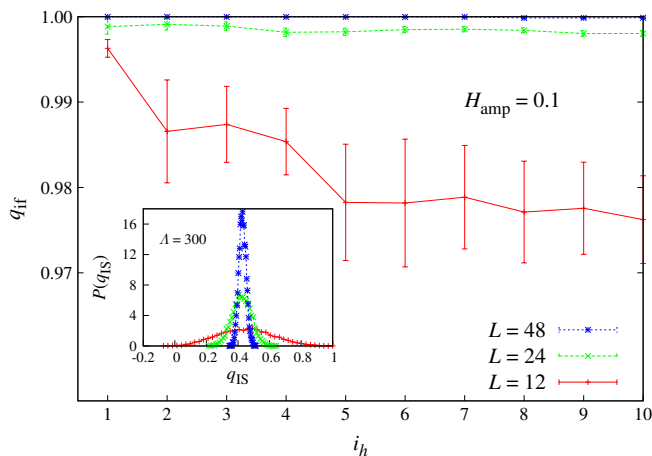


Figure 3. Overlap q_{if} between initial and forced IS (if another IS is reached) as a function of the forcing step i_h for $H_{amp} = 0.1$, for forcing along the softest mode. The inset shows the distribution of the overlaps of randomly found ISs.

$|\text{IS}^*\rangle = |\vec{s}^{(\text{IS})}\rangle$, the second minimization lead the system back to its original configuration, so the forcing was too weak to break through an energy barrier. On the contrary, if $|\text{IS}^*\rangle \neq |\vec{s}^{(\text{IS})}\rangle$ the forcing was large enough for a hop to another valley.

To ensure well-defined forcings along $|\vec{\pi}_{\text{RAND}}\rangle$, we normalize A_F with $\|\vec{\pi}\|_1 = \sum_{\mathbf{x}} |\vec{\pi}_{\mathbf{x}}|$. Indeed, the perturbation in (3) is bounded by $|\sum_{\mathbf{x}} \vec{\pi}_{\mathbf{x}} \cdot \vec{s}_{\mathbf{x}}| \leq |\sum_{\mathbf{x}} \vec{\pi}_{\mathbf{x}} \cdot \vec{s}_{\mathbf{x}}| \leq \|\vec{\pi}\|_1$. So, the perturbation is made extensive by choosing $A_F = \mathcal{A}i_h$, with $\mathcal{A} = \frac{NA}{\|\vec{\pi}\|_1}$, where the amplitudes A are an external parameter (of order 1), that we tuned in order to be in the linear response regime for small i_h , and just out of it for i_h approaching N_F (see appendix).

For the softest mode we analyzed the effect of forcings of order $O(1)$ because larger ones lead the system out of the linear response regime, so the amplitude of the forcings along $|\pi_0\rangle$ is $A_F(i_h) = \frac{Ai_h}{\|\vec{\pi}\|_1}$.

See the appendices for further details about the linear-response regime, hops between valleys and the phenomenology of these rearrangements.

Two-level systems In the spectrum of \mathcal{M} , $\rho(\lambda)$, there is an extensive number of very soft modes, with a localized eigenstate. The eigenstates can connect different ISs through the forcing procedure we described. The connection caused by such states is privileged, because the couples of ISs are very similar one to the other. We show this in figure 3, where we compare the overlap q_{if} between the configurations obtained through a forcing of amplitude $A_F(i_h)$ with the typical overlap between independent ISs.⁵ This happens for every field that produces

⁵ The overlap q_{if} between $|\vec{s}^{(\text{IS})}\rangle$ and $|\text{IS}(i_h)\rangle$ is defined as $q_{if} \equiv \frac{1}{N} \sum_{\mathbf{x}} q_{if,\mathbf{x}}$, with $q_{if,\mathbf{x}} = \vec{s}_{\mathbf{x}}^{(\text{IS})} \cdot \vec{s}_{\mathbf{x}}(i_h)$, being $\vec{s}_{\mathbf{x}}(i_h)$ the spins of the configuration $|\text{IS}(i_h)\rangle$.

rearrangements (at $H_{amp} = 10, 50$ the energy landscape is too trivial and the forcings never lead to a new IS), as it can be seen from Fig. 4, top, where we show only the overlap q_{if} with the largest forcings, of $i_h = 10$. We plot $1 - q_{if}$ and put it on log-scale so it is better visible. The

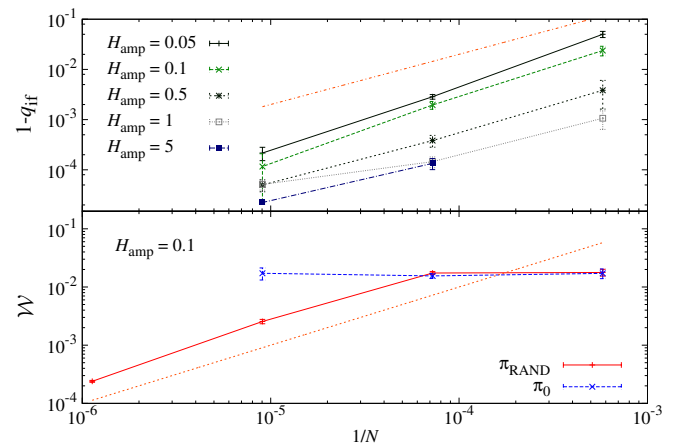


Figure 4. Top: $1 - q_{if}$ for rearrangements that occurred at the 10^{th} forcing step, for fields $H_{amp} = 0.05, 0.1, 0.5, 1, 5$. Bottom: cumulant \mathcal{W} as a function of $1/N$ for $|\vec{\pi}_{\text{RAND}}\rangle$ and $|\vec{\pi}_0\rangle$. In both plots, the straight line is a reference curve $\propto 1/N$.

overlaps q_{if} are much closer to 1 than the overlaps of independent ISs (Fig. 3, inset). This means that the ISs are somewhat clustered in tiny groups that are represented by a single IS. This could be an operational definition of classical TLS, i.e. a system in which there are two very close states, where the transitions from one state to the other can be treated as independent of the rest of the system [42–46].

Moreover, the energy barriers separating these privileged states are positive, but they do not grow with the system size (see figure 14 in the appendix). This suggests that in the thermodynamic limit $|\text{IS}^*\rangle$ and $|\vec{s}^{(\text{IS})}\rangle$ are separated by an infinitely small energy barrier, just as in a TLS.

We can get more insight on the type of rearrangement that took place during the valley change, by defining the cumulant $\mathcal{W} = \frac{\sum_{\mathbf{x}} w_{\mathbf{x}}^2}{(\sum_{\mathbf{x}} w_{\mathbf{x}})^2}$, where $w_{\mathbf{x}} = 1 - q_{if,\mathbf{x}}$. If the rearrangement is completely localized, $\mathcal{W} = 1$, whereas if it is maximally delocalized $\mathcal{W} = 1/N$. Fig 4, bottom, shows that, as expectable, the rearrangements are localized when we stimulate the system along the softest mode, and delocalized when it is along a random direction.

Conclusions The introduction of a random field in the Heisenberg spin glass model, besides extinguishing the rotational symmetry, changes qualitatively the shape of its DOS. Very strong random fields suppress the soft modes, and a gap appears in the DOS $g(\omega)$. Still, soft modes do resist the application of a random field when

it is not too large. The data are compatible with the absence of a gap, where for small ω the DOS grows as $g(\omega) \propto \omega^4$, differently from the zero-field expectation, $g(\omega) \propto \omega^2$ [13, 21].

It appears that a finite fraction of the modes is localized, suggesting a localization transition when the system becomes large.

We also analyzed the anharmonicity of the energy landscape, by imposing an external force on the system. The reaction of the spin glass has a strong dependency on the direction of application of the force. Forcings along a random direction, need to be extensively strong in order to move the orientation of the spins. Equivalent results, instead, can be obtained through forcings of order 1, if they are oriented along the softest mode.

Forcings along the softest mode cause localized rearrangements that lead the system to a new IS that is infinitely similar to the original one. The two states are separated by very small energy barriers. This could be used as an operational definition of classical TLSs.

We were supported by the European Research Council under the European Union's Seventh Framework Programme (FP7/2007-2013, ERC grant agreement no. 247328). We were partly supported by MINECO, Spain, through the research contract N^o. FIS2012-35719-C02. This work was partially supported by the GDRE 224 CNRS-INdAM GREFI-MEFI. M.B.-J. was supported by the FPU program (Ministerio de Educación, Spain). The authors thankfully acknowledge the resources from the supercomputer "Memento", technical expertise and assistance provided by BIFI-ZCAM (Universidad de Zaragoza).

Appendix

Parameters of the simulations

In Tab. I we resume how many samples we simulated for each couple (L, H) both for the spectrum $\rho(\lambda)$, and for the forcings, the number of eigenvalues n_λ that was computed with Arpack, and the amplitudes A of the forcings.

Reaching the inherent structure

As energy minimization algorithm we use the successive overrelaxation, that was successfully used in [47] for 3d Heisenberg spin glasses. It consists in an interpolation, through a parameter Λ , between a direct quench, that aligns all the spins to the local field \vec{h}_x (see. e.g. [48] for a recent application in Heisenberg spin glasses), and the microcanonical overrelaxation update (well explained in [49]).

H_{amp}	L	n_{samples}	n_{replicas}	n_λ	$A(\vec{\pi}_0\rangle)$	$A(\vec{\pi}_{\text{RAND}}\rangle)$
50	192	10 (0)	2	35	-	-
50	96	10 (10)	2	80	-	1
50	48	70 (70)	2	500	1	1
50	24	100 (100)	2	500	1	1
50	12	100 (100)	2	500	1	1
10	192	10 (0)	2	35	-	-
10	96	10 (10)	2	80	-	0.72
10	48	70 (70)	2	500	0.6	0.72
10	24	100 (100)	2	500	0.3	0.72
10	12	100 (100)	2	500	0.3	0.72
5	192	10 (0)	2	35	-	-
5	96	10 (10)	2	80	-	0.3
5	48	70 (70)	2	500	0.014	0.3
5	24	100 (100)	2	500	0.02	0.3
5	12	100 (100)	2	500	0.024	0.3
1	192	10 (0)	2	35	-	-
1	96	10 (10)	2	80	-	0.05
1	48	70 (70)	2	500	0.004	0.05
1	24	100 (100)	2	500	0.0045	0.05
1	12	100 (100)	2	500	0.0045	0.05
0.5	192	10 (0)	2	35	-	-
0.5	96	10 (10)	2	80	-	0.022
0.5	48	70 (70)	2	500	0.008	0.02
0.5	24	100 (100)	2	500	0.009	0.022
0.5	12	100 (100)	2	500	0.009	0.022
0.1	192	10 (0)	2	35	-	-
0.1	96	10 (10)	2	80	-	0.012
0.1	48	100 (70)	2	500	0.006	0.012
0.1	24	100 (100)	2	500	0.1	0.012
0.1	12	100 (100)	2	500	0.1	0.012
0.05	192	10 (0)	2	35	-	-
0.05	96	10 (10)	2	80	-	0.011
0.05	48	100 (70)	2	500	0.06	0.011
0.05	24	100 (100)	2	500	0.42	0.011
0.05	12	100 (100)	2	500	0.36	0.011
0.01	192	10 (0)	2	25	-	-
0.01	96	10 (10)	2	80	-	0.016
0.01	48	100 (70)	2	500	0.045	0.016
0.01	24	100 (100)	2	500	0.009	0.004
0.01	12	100 (100)	2	500	0.007	0.001

Table I. Samples and replicas of our simulations. The number between parenthesis is the amount of samples used for the forcings. We indicate with n_λ the number of eigenvalues we calculated from the bottom of the spectrum $\rho(\lambda)$. $A(|\vec{\pi}_{\text{RAND}}\rangle)$ and $A(|\vec{\pi}_0\rangle)$ are the forcings' parameters.

We propose sequential single-flip updates with the rule

$$\vec{s}_x^{\text{SOR}} = \frac{\vec{h}_x + \Lambda \vec{s}_x^{\text{OR}}}{\|\vec{h}_x + \Lambda \vec{s}_x^{\text{OR}}\|}, \quad (4)$$

where \vec{s}_x^{OR} is the overrelaxation update

$$\vec{s}_x^{\text{OR}} = 2\vec{h}_x \frac{\vec{h}_x \cdot \vec{s}_x^{\text{old}}}{h_x^2} - \vec{s}_x^{\text{old}}. \quad (5)$$

The limit $\Lambda = 0$ corresponds to a direct quench that notoriously presents convergence problems. On the other side, with $\Lambda = \infty$ the energy does not decrease.

It is shown in [47] that the optimal value of Λ in terms of convergence speed is $\Lambda \approx 300$. Thus, the search of ISs was done with $\Lambda = 300$, under the reasonable assumption, that we will reinforce right away, that a change on Λ does not imply sensible changes in the observables we examine. In fact, the concept of IS is strictly related to the protocol one chooses to relax the system, and on the starting configuration. From [47] our intuition is that despite the ISs' energies do depend on these two elements, this dependency is small and we can neglect it (dependencies on the correlation lengths will be examined in a future work [33]).

To validate the generality of our results we compared the ISs reached with $\Lambda = 300, 1, 0$, at $H_{\text{amp}} = 0$ over a wide range of temperatures. We took advantage, for this comparison, of the $L = 48$ configurations that were thermalized in [50], that go from T_{SG} to $\frac{5}{3}T_{\text{SG}}$.

In figure 5 we plot the energy E_{IS} of the reached ISs,⁶ as a function of the temperature T . We show ten random samples, each minimized with $\Lambda = 300, 1, 0$. Increasing Λ the energy of the inherent structures decreases but this variation is smaller than the dispersion between different samples. The energy of the ISs also decreases with T , but this decrease too is smaller than the fluctuation between samples. Since the dispersion on the energy is dominated

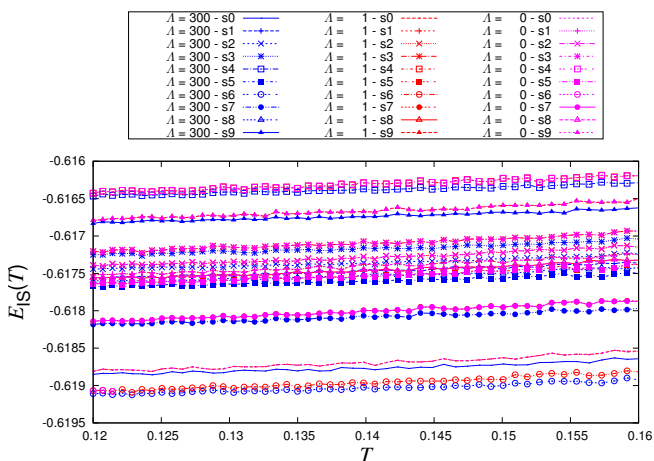


Figure 5. Energy of the inherent structure as a function of temperature for 10 samples chosen at random, for $H_{\text{amp}} = 0$, $L = 48$. We use the same symbol for the same sample. ISs obtained with $\Lambda = 300$ are in blue, red represents $\Lambda = 1$ and purple stands for $\Lambda = 0$. Purple and red lines almost overlap. Sample-to-sample fluctuations are the largest source of dispersion, compared with Λ and T .

by the disorder, rather than by Λ or T , we can think of putting ourselves in the most convenient situation: $T = \infty$, that does not require thermalization, and $\Lambda = 300$, that yields the fastest minimization.

Also the spectrum of the dynamical matrix does not show relevant signs of dependency on either T of Λ , as shown in figure 6.

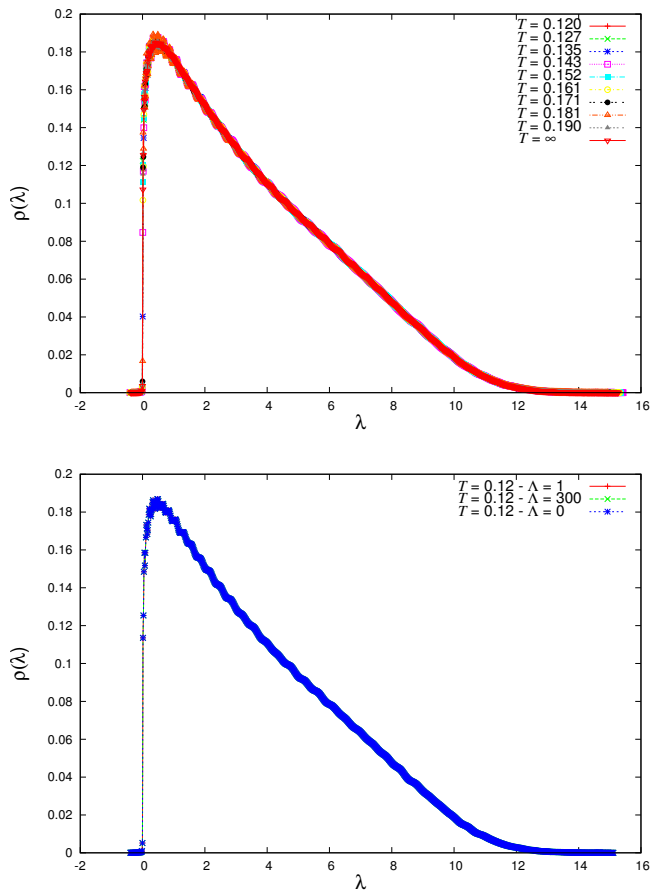


Figure 6. Spectrum $\rho(\lambda)$ of the Hessian matrix calculated at the inherent structure for $H_{\text{amp}} = 0$, $L = 48$, with the method of the moments. **Top:** $\rho(\lambda)$ for different temperatures from $T = 0.12$ to $T = \infty$. **Bottom:** comparison of the spectrum between $\Lambda = 1$ and $\lambda = 300$ at $T = 0.12, 0.19, \infty$ various Λ .

⁶ With a normalization factor $1/3N$ that bounds it to unity.

The Dynamical matrix

We calculate the dynamical matrix as the Hessian matrix \mathcal{M} of Hamiltonian

$$\mathcal{H}_{\text{RF}}(|\vec{s}\rangle) = - \sum_{|\mathbf{x}-\mathbf{y}|=1} J_{\mathbf{x}\mathbf{y}} \vec{s}_{\mathbf{x}} \cdot \vec{s}_{\mathbf{y}} - \sum_{\mathbf{x}} \vec{h}_{\mathbf{x}} \cdot \vec{s}_{\mathbf{x}}, \quad (6)$$

calculated at the local minima of the energy. It is not straightforward to compute \mathcal{M} because it is necessary to take in account the normalization of the spins $\vec{s}_{\mathbf{x}}^2 = 1 \forall \mathbf{x}$.

To this scope we define local perturbation vectors $\vec{\pi}_{\mathbf{x}}$, called pions in analogy with the nonlinear σ model [51]. The distinguishing feature of the pions is that they are orthogonal to the IS, $(\vec{s}_{\mathbf{x}} \cdot \vec{\pi}_{\mathbf{x}}) = 0$, and that their global norm is unitary, $\langle \vec{\pi} | \vec{\pi} \rangle = 1$, where $\langle \vec{a} | \vec{b} \rangle$ indicates the scalar product between configurations, $\langle \vec{a} | \vec{b} \rangle \equiv \sum_{\mathbf{x}} \vec{a}_{\mathbf{x}} \cdot \vec{b}_{\mathbf{x}}$.

We use the pions to parametrize order ϵ perturbations around the IS as

$$\vec{s}_{\mathbf{x}}^{\epsilon} = \vec{s}_{\mathbf{x}}^{(\text{IS})} \sqrt{1 - \epsilon^2 \vec{\pi}_{\mathbf{x}}^2} + \epsilon \vec{\pi}_{\mathbf{x}}, \quad (7)$$

so the position of $\vec{s}_{\mathbf{x}}^{\epsilon}$ is fully determined by $\vec{\pi}_{\mathbf{x}}$. As long as ϵ is small enough to grant $\epsilon^2 \vec{\pi}_{\mathbf{x}}^2 < 1 \forall \mathbf{x}$, the normalization condition is naturally satisfied without the need to impose any external constraint.

We now build a local reference change. For each site \mathbf{x} we define a local basis $\mathcal{B} = \left\{ \vec{s}_{\mathbf{x}}^{(\text{IS})}, \hat{e}_{1,\mathbf{x}}, \hat{e}_{2,\mathbf{x}} \right\}$, where $\hat{e}_{1,\mathbf{x}}, \hat{e}_{2,\mathbf{x}}$ are any two unitary vectors, orthogonal to each other and to $\vec{s}_{\mathbf{x}}^{(\text{IS})}$, and well oriented. In our simulations they were generated randomly. In this basis the pions can be rewritten as $\vec{\pi}_{\mathbf{x}} = (0, a_1, a_2)$, where now they explicitly depend only on two components, with real values a_1 and a_2 . We can therefore rewrite the pions as two-component vectors $\vec{\pi}_{\mathbf{x}} = (a_1, a_2)$. At this point we integrated the normalization constraint with the parametrization, and we can obtain the $2N \times 2N$ Hessian matrix \mathcal{M} , that acts on $2N$ -component vectors $|\vec{\pi}\rangle$, by a second-order development of \mathcal{H}_{IS} (the derivation of \mathcal{M} is shown in the subsection ahead). The obtain matrix is sparse, with 13 non-zero elements per line (1 diagonal element, and 6 two-component vectors for the nearest-neighbors). The matrix element $\mathcal{M}_{\mathbf{x}\mathbf{y}}^{\alpha\beta}$ is

$$\mathcal{M}_{\mathbf{x}\mathbf{y}}^{\alpha\beta} = \mathcal{M}_{\mathbf{x}\mathbf{y}}(\hat{e}_{\alpha,\mathbf{x}} \cdot \hat{e}_{\beta,\mathbf{y}}), \quad (8)$$

with

$$\mathcal{M}_{\mathbf{x}\mathbf{y}} = \delta_{\mathbf{x}\mathbf{y}} (\vec{h}_{\mathbf{y}}^{(\text{IS})} \cdot \vec{s}_{\mathbf{y}}^{(\text{IS})}) - \sum_{\mu=-D}^D J_{\mathbf{x}\mathbf{y}} \delta_{\mathbf{x}+\hat{\mu},\mathbf{y}}, \quad (9)$$

where the bold arab characters indicate the site, and the greek characters indicate the component of the two-dimensional vector.

Derivation of the expression for the Hessian

We derive the expression of the Hessian matrix \mathcal{M} of the Hamiltonian \mathcal{H}_{RF} [eq. (6 in the main article)] that we implemented in our programs.

In terms of pionic perturbations [recall eq. (7)], \mathcal{M} would be defined as $\mathcal{M}_{\mathbf{x}\mathbf{y}}^{\alpha\beta} = \frac{\partial^2 \mathcal{H}_{\text{RF}}}{\partial \pi_{\mathbf{x},\alpha} \partial \pi_{\mathbf{y},\beta}}$. An easy way to extract the Hessian is to write \mathcal{H}_{RF} as perturbations around the IS and to pick only the second-order terms.

To rewrite \mathcal{H}_{RF} as a function of the pionic perturbations, it is simpler to compute separately the dot products $(\vec{s}_{\mathbf{x}} \cdot \vec{s}_{\mathbf{y}})$ and $\vec{h}_{\mathbf{x}} \cdot \vec{s}_{\mathbf{x}}$. Including the ϵ factors into the perturbation π_x , the generic spin near the IS is expressed as $\vec{s}_{\mathbf{x}} = \vec{s}_{\mathbf{x}}^{(\text{IS})} \sqrt{1 - \vec{\pi}_{\mathbf{x}}^2} + \vec{\pi}_{\mathbf{x}}$. We can make a second-order expansion of the non-diagonal part of the Hamiltonian by taking the first-order expansion of the square root $\sqrt{1 - \vec{\pi}_{\mathbf{x}}^2} \simeq 1 - \vec{\pi}_{\mathbf{x}}^2/2$,

$$\begin{aligned} (\vec{s}_{\mathbf{x}} \cdot \vec{s}_{\mathbf{y}}) &= \quad (10) \\ &= \left(\vec{s}_{\mathbf{x}}^{(\text{IS})} \sqrt{1 - \vec{\pi}_{\mathbf{x}}^2} + \vec{\pi}_{\mathbf{x}} \right) \cdot \left(\vec{s}_{\mathbf{y}}^{(\text{IS})} \sqrt{1 - \vec{\pi}_{\mathbf{y}}^2} + \vec{\pi}_{\mathbf{y}} \right) = \\ &= \left(\vec{s}_{\mathbf{x}}^{(\text{IS})} \cdot \vec{s}_{\mathbf{y}}^{(\text{IS})} \right) + \left(\vec{s}_{\mathbf{x}}^{(\text{IS})} \cdot \vec{\pi}_{\mathbf{y}} \right) + \left(\vec{s}_{\mathbf{y}}^{(\text{IS})} \cdot \vec{\pi}_{\mathbf{x}} \right) + \\ &+ \frac{1}{2} \left[(-\vec{\pi}_{\mathbf{x}}^2 - \vec{\pi}_{\mathbf{y}}^2) \left(\vec{s}_{\mathbf{x}}^{(\text{IS})} \cdot \vec{s}_{\mathbf{y}}^{(\text{IS})} \right) + 2\vec{\pi}_{\mathbf{x}} \cdot \vec{\pi}_{\mathbf{y}} \right] + o(\vec{\pi}^3). \end{aligned}$$

On the other hand the random-field term is

$$\begin{aligned} (\vec{h}_{\mathbf{x}} \cdot \vec{s}_{\mathbf{x}}) &= \vec{h}_{\mathbf{x}} \cdot \left(\vec{s}_{\mathbf{x}}^{(\text{IS})} \sqrt{1 - \vec{\pi}_{\mathbf{x}}^2} + \vec{\pi}_{\mathbf{x}} \right) = \quad (11) \\ &= \left(\vec{h}_{\mathbf{x}} \cdot \vec{s}_{\mathbf{x}}^{(\text{IS})} \right) + \left(\vec{h}_{\mathbf{x}} \cdot \vec{\pi}_{\mathbf{x}} \right) - \frac{\vec{\pi}_{\mathbf{x}}^2}{2} \left(\vec{h}_{\mathbf{x}} \cdot \vec{s}_{\mathbf{x}}^{(\text{IS})} \right) + o(\vec{\pi}^3). \end{aligned}$$

By inserting eqs.(10,11) and taking only the second-order terms we obtain how the Hessian matrix acts on the fields $|\vec{\pi}\rangle$:

$$\begin{aligned} \frac{1}{2} \langle \vec{\pi}_{\mathbf{x}} | \mathcal{M} | \vec{\pi}_{\mathbf{y}} \rangle &= \quad (12) \\ &= -\frac{1}{2} \sum_{\langle \mathbf{x}, \mathbf{y} \rangle} J_{\mathbf{x}, \mathbf{y}} \left[(-\vec{\pi}_{\mathbf{x}}^2 - \vec{\pi}_{\mathbf{y}}^2) \left(\vec{s}_{\mathbf{x}}^{(\text{IS})} \cdot \vec{s}_{\mathbf{y}}^{(\text{IS})} \right) + \right. \\ &\quad \left. + 2\vec{\pi}_{\mathbf{x}} \cdot \vec{\pi}_{\mathbf{y}} \right] + \sum_{\mathbf{x}} \frac{\vec{\pi}_{\mathbf{x}}^2}{2} \left(\vec{h}_{\mathbf{x}} \cdot \vec{s}_{\mathbf{x}}^{(\text{IS})} \right) = \\ &= \frac{1}{2} \sum_{\mathbf{x}} \vec{\pi}_{\mathbf{x}}^2 \left[\vec{s}_{\mathbf{x}}^{(\text{IS})} \cdot \left(\vec{h}_{\mathbf{x}}^{(\text{IS})} + \vec{h}_{\mathbf{x}} \right) \right] + \\ &\quad + \frac{1}{2} \sum_{\mathbf{x}} \vec{\pi}_{\mathbf{x}} \cdot \sum_{\mathbf{y}:|\mathbf{x}-\mathbf{y}|=1} J_{\mathbf{x}\mathbf{y}} \vec{\pi}_{\mathbf{y}}, \end{aligned}$$

where we called $\vec{h}_{\mathbf{x}}^{(\text{IS})}$ the local field of the IS. The just-obtained expression represents a sparse matrix with a matrix element $\mathcal{M}_{\mathbf{x}\mathbf{y}}$ that comfortably splits as $\mathcal{M}_{\mathbf{x}\mathbf{y}} =$

$\mathcal{D}_{\mathbf{x}\mathbf{y}} + \mathcal{N}_{\mathbf{x}\mathbf{y}}$ into a diagonal term $\mathcal{D}_{\mathbf{x}\mathbf{y}}$ and a nearest-neighbor one $\mathcal{N}_{\mathbf{x}\mathbf{y}}$, with

$$\mathcal{D}_{\mathbf{x}\mathbf{y}} = \delta_{\mathbf{x}\mathbf{y}} \left[\vec{s}_{\mathbf{x}}^{(\text{IS})} \cdot \left(\vec{h}_{\mathbf{x}}^{(\text{IS})} + \vec{h}_{\mathbf{x}} \right) \right], \quad (13)$$

$$\mathcal{N}_{\mathbf{x}\mathbf{y}} = - \sum_{\mu=-d}^d J_{\mathbf{x}\mathbf{y}} \delta_{\mathbf{x}+\hat{e}_{\mu},\mathbf{y}}, \quad (14)$$

where \hat{e}_{μ} is the unit vector towards one of the $2d$ neighbors.

\mathcal{M} in the local reference frame The last step is to get an expression of the Hessian matrix in the local reference frame, that includes the spin normalization constraint.

In the local reference frame the pions are written like $\vec{\pi} = a_1 \hat{e}_{1,\mathbf{x}} + a_2 \hat{e}_{2,\mathbf{x}}$ because they are perpendicular to the first vector of the basis, $\vec{s}_{\mathbf{x}}^{(\text{IS})}$, and that is why we write them in a two-dimensional representation as $\vec{\pi} = (a_1, a_2)$.

In this local basis, the matrix element acting on the pions is written as

$$\vec{\pi}_{\mathbf{x}} \mathcal{M}_{\mathbf{x}\mathbf{y}} \vec{\pi}_{\mathbf{y}} = \vec{\pi}_{\mathbf{x}} \mathcal{M}_{\mathbf{x}\mathbf{y}} \vec{\pi}_{\mathbf{y}} = \quad (15)$$

$$= (a_{1,\mathbf{x}}, a_{2,\mathbf{x}}) \begin{pmatrix} \mathcal{M}_{\mathbf{x}\mathbf{y}}(\hat{e}_{1,\mathbf{x}} \cdot \hat{e}_{1,\mathbf{y}}) & \mathcal{M}_{\mathbf{x}\mathbf{y}}(\hat{e}_{2,\mathbf{x}} \cdot \hat{e}_{1,\mathbf{y}}) \\ \mathcal{M}_{\mathbf{x}\mathbf{y}}(\hat{e}_{1,\mathbf{x}} \cdot \hat{e}_{2,\mathbf{y}}) & \mathcal{M}_{\mathbf{x}\mathbf{y}}(\hat{e}_{2,\mathbf{x}} \cdot \hat{e}_{2,\mathbf{y}}) \end{pmatrix} \begin{pmatrix} a_{1,\mathbf{y}} \\ a_{2,\mathbf{y}} \end{pmatrix},$$

so in the $2N$ -dimensional reference \mathcal{M} is expressed as

$$\mathcal{M}_{\mathbf{x}\mathbf{y}}^{\alpha\beta} = \mathcal{M}_{\mathbf{x}\mathbf{y}}(\hat{e}_{\alpha,\mathbf{x}} \cdot \hat{e}_{\beta,\mathbf{y}}), \quad (16)$$

and the elements of the diagonal and nearest-neighbor operators \mathcal{D} and \mathcal{N} become

$$\mathcal{D}_{\mathbf{x}\mathbf{y}}^{\alpha\beta} = \delta_{\mathbf{x}\mathbf{y}} \delta^{\alpha\beta} \left[\vec{s}_{\mathbf{x}}^{(\text{IS})} \cdot \left(\vec{h}_{\mathbf{x}}^{(\text{IS})} + \vec{h}_{\mathbf{x}} \right) \right], \quad (17)$$

$$\mathcal{N}_{\mathbf{x}\mathbf{y}}^{\alpha\beta} = - \sum_{\mu=-d}^d J_{\mathbf{x}\mathbf{y}} \delta_{\mathbf{x}+\hat{e}_{\mu},\mathbf{y}} (\hat{e}_{\alpha,\mathbf{x}} \cdot \hat{e}_{\beta,\mathbf{y}}). \quad (18)$$

Cumulatives for all the fields

To calculate $F(\lambda)$, for numerical purposes we compute the average of the k^{th} eigenvalue, and we plot $k/(2N)$ versus $\langle \lambda_k \rangle$. In this way we deliberately avoid to looking to the tail in $F(\lambda)$ that in finite volume systems is present as an effect of the fluctuation of the lowest eigenvalues. With these procedure the errorbars are on the x axis. An advantage is that the function $F(\lambda)$ does not depend on the number of eigenvalue computed.

In figures 7 and 8 we show the function $F(\lambda)$ for all the fields we simulated. We were able to calculate with Arpack the lowest eigenvalues of the spectrum. The number of calculated eigenvalues n_{λ} is in table I. All the plots are compared with the Debye behavior $\lambda^{1.5}$ and with the power law behavior $\lambda^{2.5}$, because our data suggest that a universality on the exponents would set them around $\gamma = 2.5$, $\delta = 4$ and $\alpha = 1.5$. This is straightforward for $H_{\text{amp}} = 0.1, 0.5, 1, 5$, where when λ is small

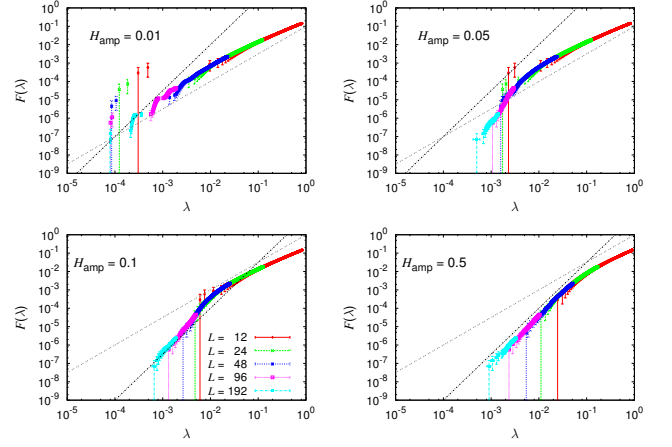


Figure 7. Cumulative distributions $F(\lambda)$ for small random fields $H_{\text{amp}} = 0.01, 0.05, 0.1, 0.5$. In each plot we show black a reference curve representing the power law $\lambda^{2.5}$, that is our guess for a universal behavior, and a grey line indicating the Debye behavior $\lambda^{1.5}$. One could expect a Debye behavior for $\lambda > \lambda^*$, with $\lambda^* \rightarrow 0$ as $H_{\text{amp}} \rightarrow 0$. Instead, we see an excess of eigenvalues even compared to the Debye behavior, indicating a likely boson peak. Further discussions in the main text.

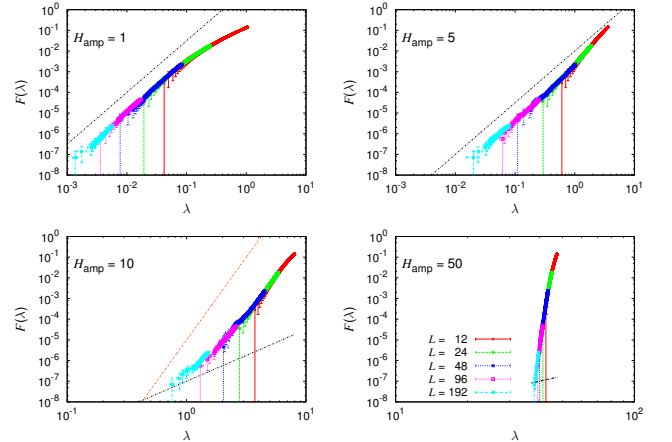


Figure 8. Cumulative distributions $F(\lambda)$ for large random fields $H_{\text{amp}} = 1, 5, 10, 50$. In each plot we show a reference curve representing the power law $\lambda^{2.5}$. The orange line in the bottom left set is proportional to λ^8 .

there is a clear power law behavior, with a power close to 2.5, while it can be excluded for $H_{\text{amp}} = 50$, where the soft modes are suppressed in favor of a gap, as it was also visible from the inset of figure 1 of the main article. At $H_{\text{amp}} = 10$ we are probably close to where the gap forms. The $F(\lambda)$ goes as a large power law λ^8 when λ is large, but at the smallest values of λ , recovered from $L = 192$, there is a slight change of power law towards something that could become 2.5. One could also argue that a $F(\lambda)$ goes to zero as a power law for any finite H_{amp} , as long as one looks at small enough λ . Numerical

analysis cannot answer to questions of this type, but still, even if no sharp transition is present, an empirical gap is clearly present for large H_{amp} , since the precision of any experiment (numerical or real) is finite. In the case of the smallest fields $H_{\text{amp}} = 0.01, 0.05$, we suffer from effects from $H_{\text{amp}} = 0$. The spin waves do not hybridize with the bulk of the spectrum, and pseudo-Goldstone modes with a very small eigenvalue appear, making it hard to extract a power law behavior.

Overall, we see good evidence for a γ around 2.5 at several values of H_{amp} , and at other fields the data is not in contradiction with a hypothesis of universality in the exponents defined by

$$g(\omega) \sim \omega^\delta, \quad \rho(\lambda) \sim \lambda^\alpha, \quad F(\lambda) \sim \lambda^\gamma. \quad (19)$$

When the field is small we remark a change of trend from $\gamma \approx 2.5$ to $\gamma < 1.5$ at a value λ^* . The crossover λ^* shifts towards zero as H_{amp} decreases. This probably indicates the presence of a boson peak, an excess of modes at low frequency. Signs of a boson peak in at $H_{\text{amp}} = 0$ can be seen in figure 6. In that case the mass of the spectrum is all concentrated at low λ , but there ought to be a Debye behavior, meaning that λ^* is very little.

Eigenvector correlation function

Since in a localized state the eigenvectors have a well-defined correlation length, we can use also this criterion to probe the localization. We can define a correlation length from Green's function \mathcal{G} , that is defined through the relation $\mathcal{M}\mathcal{G} = \delta_{\mathbf{x}\mathbf{y}}$, an is commonly used in field theory for two-point correlations. Since \mathcal{M}^{-1} shares eigenvectors $|\psi_n\rangle$ with \mathcal{M} and has inverse eigenvalues $1/\lambda_n$, Green's function is ⁷

$$\mathcal{G}(\mathbf{x}, \mathbf{y}) = \mathcal{M}^{-1}\delta_{\mathbf{x}\mathbf{y}} = \sum_n \frac{\psi_n(\mathbf{x})\psi_n(\mathbf{y})}{\lambda_n}, \quad (20)$$

and squaring the relation

$$\mathcal{G}^2(\mathbf{x}, \mathbf{y}) = \sum_{m,n} \frac{\psi_m(\mathbf{x})\psi_m(\mathbf{y})\psi_n(\mathbf{x})\psi_n(\mathbf{y})}{\lambda_m\lambda_n}. \quad (21)$$

By averaging over the disorder we gain translational invariance and $\overline{\mathcal{G}^2}$ can be written as a function of the distance $\mathbf{r} = \mathbf{x} - \mathbf{y}$,

$$\overline{\mathcal{G}^2(\mathbf{r})} = \sum_{m,n} \frac{1}{\lambda_m\lambda_n} \sum_{\mathbf{x}} \left(\frac{[\psi_m(\mathbf{x})\psi_n(\mathbf{x})][\psi_m(\mathbf{x}+\mathbf{r})\psi_n(\mathbf{x}+\mathbf{r})]}{V} \right). \quad (22)$$

⁷ For simplicity we use N -component eigenvectors $\psi_n(\mathbf{x})$ instead of the $2N$ -component ones $|\vec{\pi}\rangle$. The relationship between the two can be recovered through $\psi_n^2(\mathbf{x}) = \vec{\pi}^2 = \pi^2$.

Making the reasonable assumption that different eigenvectors do not interfere with each other, and exploiting the orthogonality condition $\sum_{\mathbf{x}} \psi_m(\mathbf{x})\psi_n(\mathbf{x}) = \delta_{mn}$, we obtain the desired correlation function

$$\mathcal{C}(\mathbf{r}) = \overline{\mathcal{G}^2(\mathbf{r})} = \sum_n \frac{1}{\lambda_n^2} \overline{\psi_n^2(\mathbf{x})\psi_n^2(\mathbf{x}+\mathbf{r})}. \quad (23)$$

This correlation function favors the softest modes by a factor $1/\lambda_n^2$. This is an advantage, because the bulk modes do not exhibit a finite correlation length, so it is useful to have them suppressed.

The correlation function for small fields

As we show in Fig. 9, when H_{amp} is small the correlation function is not exponential.

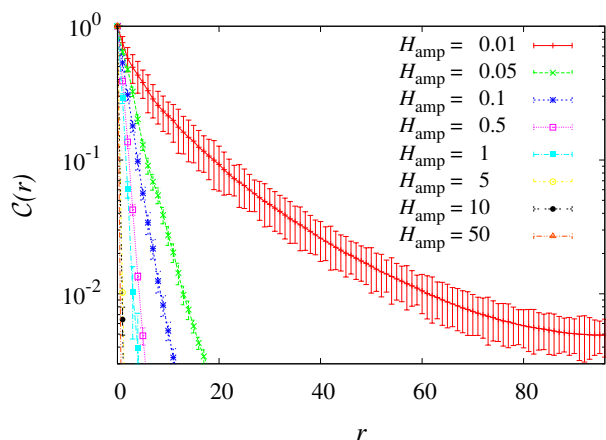


Figure 9. The correlation function $\mathcal{C}(r)$ extracted from the eigenvectors in $L = 192$ lattices.

Forcings

Probing the linear regime

To make sure that our forcings are not too strong, we monitor the direct reaction of the system to the forcing. We define a “polarized magnetization” $\hat{m} = \langle \text{IS}(i_h) | \vec{\pi} \rangle = \sum_{\mathbf{x}} \vec{s}_{\mathbf{x}} \cdot \pi_{\mathbf{x}}$, that indicates how much the forcing pushed the alignment of the spins along the pion. The amplitude of the forcing is tuned well if $\hat{m}(i_h)$ is close to the linear regime. In table I we show the amplitudes A we used in order to be in the linear regime. Figure 10 confirms that this was the working condition for the forcings along $|\vec{\pi}_0\rangle$. Figure 11 is analogous, but along $|\vec{\pi}_{\text{RAND}}\rangle$. In the latter figure we rescale \hat{m} by a factor $1/\sqrt{N}$ to obtain a collapse. In fact the normalization $\langle \vec{\pi}_{\text{RAND}} | \vec{\pi}_{\text{RAND}} \rangle = 1$ implies that the components of $|\vec{\pi}_{\text{RAND}}\rangle$ are of order

$1/\sqrt{N}$, so the polarized magnetization is bounded by $|\hat{m}| = |\langle IS(i_h) | \vec{\pi}_{\text{RAND}} \rangle| \leq \sum_{\mathbf{x}} |\vec{\pi}_{\mathbf{x}}| \sim \sqrt{N}$.

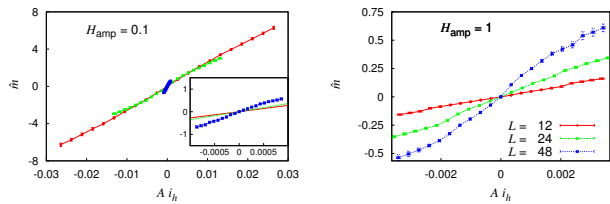


Figure 10. Polarized magnetization \hat{m} of the forcings along $|\vec{\pi}_0\rangle$, for $H_{\text{amp}} = 0.1$ (left) and $H_{\text{amp}} = 1$ (right). The inset is a zoom of the same data.

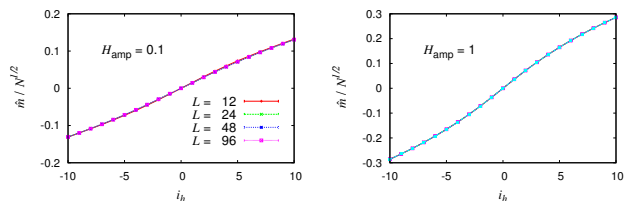


Figure 11. Rescaled polarized magnetization \hat{m} of the forcings along $|\vec{\pi}_{\text{RAND}}\rangle$, for $H_{\text{amp}} = 0.1$ (left) and $H_{\text{amp}} = 1$ (right). The data are rescaled in order to collapse.

Ending in a new valley. For each $A_{\text{F}}(i_h)$ we measure the overlap q_{if} between the two minimas of \mathcal{H}_{RF} , the initial IS, $|\vec{s}^{(\text{IS})}\rangle$, and the final one, $|\text{IS}^*\rangle$. Naïvely, checking that $q_{\text{if}} < 1$ in principle is a good criterion to establish whether the system escaped to another valley. We proceeded similarly, in terms of the spin variations between initial and final configuration, through the quantities

$$w_{\mathbf{x}} = 1 - \left(\vec{s}_{\mathbf{x}}^{(\text{IS})} \cdot \vec{s}_{\mathbf{x}}^{(\text{IS}^*)} \right), \quad (24)$$

$$W = \sum_{\mathbf{x}} w_{\mathbf{x}} = N - \langle \vec{s}^{(\text{IS})} | \text{IS}^* \rangle = N(1 - q_{\text{if}}), \quad (25)$$

$$\mathcal{W} = \frac{\sum_{\mathbf{x}} w_{\mathbf{x}}^2}{\left(\sum_{\mathbf{x}} w_{\mathbf{x}} \right)^2}. \quad (26)$$

The local variation $w_{\mathbf{x}}$ measures the change between the beginning and the end of the process. If the spin stayed the same then $w_{\mathbf{x}} = 0$, while if it became uncorrelated with the initial position $w_{\mathbf{x}} = 1$ in average. If one and only one spin becomes uncorrelated with its initial configuration, the variation of W is $\Delta W = 1/N$. Similar variations ΔW do not mean that one spin has decorrelated and the others have stayed the same, this is impossible because $|\vec{s}^{(\text{IS})}\rangle$ and $|\text{IS}^*\rangle$ are ISs and collective rearrangements are needed. A $\Delta W = 1/N$ means instead that the overall change is equivalent to a single spin becoming independent of its initial state. This is, for a rearrangement, the minimal change in the W that we can define.

Since the spins in our model are continuous variables, we impose $\Delta W = 1/N$ as a threshold to state whether there was or not a change of valley.

The cumulant \mathcal{W} is an indicator of the type of rearrangement that took place. If the rearrangement is completely localized (only one spin changes), $\mathcal{W} = 1$, whereas if it is maximally delocalized (all the spins have the same variation), then $\mathcal{W} = 1/N$.

Falling back in the same valley. Even though the forcing is along a definite direction, since the energy landscape is very irregular, it may happen that stronger forcings lead the system to the original valley. For example it may happen that $i_h = 2$ lead the system to a new valley, and $i_h = 3$ lead it once again to the same valley of $i_h = 1$. To exclude these extra apparent valleys we label each visited valley with its W , and assume that two valleys with the same label are the same valley. These events are not probable, and even less likely it is that this happen with two different but equally-labelled valleys, so we neglect the bias due to this unlucky possibility.

Rearrangements

To delineate the shape of the energy landscape, we want to study, for every couple (H_{amp}, L) , the probability that a forcing of amplitude A_{F} lead the system to a new valley, to distinguish the behavior of soft from bulk modes.

Furthermore, once the system made its first jump to a new valley, it is not excluded that a bigger forcing lead it to a third minimum of the energy. One can ask himself what is the probability $P_{H_{\text{amp}}, L}(A_{\text{F}}, n)$ that n new valleys are reached by forcing the system with an amplitude up to $A_{\text{F}}(i_h)$, and to try to evince a dependency on sistem size and random field. Even though n is bounded by i_h , this does not necessarily mean that if we made smaller and more numerous forcings n could not be larger. On another side, if for a certain parameter choice rearrangements are measured only for large i_h , it is reasonable to think that these represent the smallest possible forcings to fall off the IS.

To construct $P_{H_{\text{amp}}, L}(A_{\text{F}}, n)$, for every replica and sample we start from $i_h = 0$ and increase $|i_h|$ either in the positive or negative direction (the two are accounted for independently). The value we assign to $P_{H_{\text{amp}}, L}(A_{\text{F}}, n)$ is the number of systems that had n rearrangements after i_h steps, divided by the total number of forcings, that is $2N_{\text{rep}}N_{\text{sam}}$.

First rearrangement. In figure 12 we show the probability of measuring exactly n rearrangements after $i_h =$

$N_F = 10$ forcing steps.⁸ Even though both for $|\vec{\pi}_{\text{RAND}}\rangle$ and $|\vec{\pi}_0\rangle$ we are in the linear response regime, the behavior is very different between the two types of forcing. In the first case every single forcing step we impose leads the system to a new valley. In the second rearrangements are so uncommon that even though the probability of having exactly one rearrangement is finite, that of having more than one becomes negligible for large samples. It

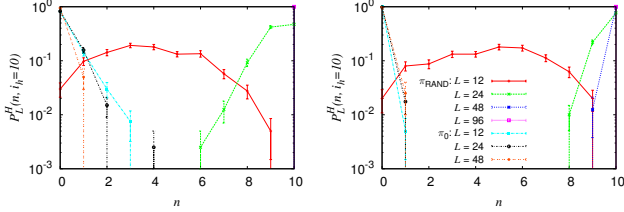


Figure 12. Probability of there being exactly n changes of valley after $i_h = N_F = 10$ forcing steps. The data come from $H_{\text{amp}} = 0.1$ (left) and $H_{\text{amp}} = 1$ (right). If $P_{H_{\text{amp}}, L}(A_F, n) = 1$ for $n = 0$ it means that the forcings were not strong enough to ever get out of the initial IS. On the contrary, $P_{H_{\text{amp}}, L}(A_F, n) = 1$ for $n = 10$ means that every single step lead the system to a new IS. The latter scenario is realized in the case of forcings along $|\vec{\pi}_{\text{RAND}}\rangle$, especially when the system size is large. On the other side, forcings along $|\vec{\pi}_0\rangle$ display a small but finite amount of rearrangements.

is then reasonable to think that any rearrangement we measure for $|\vec{\pi}_0\rangle$, it occurs for the smallest possible forcing, and even when more than one occurs, these jumps are between *neighboring valleys*, where by neighboring we mean that no smaller forcing would lead the system to a different IS. To convince ourselves of this we can give a look at the average number of rearrangements after i_h forcing steps, $n(i_h)$ (figure 13).⁹ When i_h is small no new ISs are visited and $n(i_h) = 0$, while for larger i_h , $n(i_h)$ is positive but small, so we can call these changes of valley “first rearrangements”, i.e. rearrangement between *neighboring valleys*.

Energy Barriers

To reinforce the idea of two-level system (TLS), we report the energy barriers between the couples of connected ISs. The maximum value of ΔE before a hop to another valley should give an estimate of height of

⁸ We do not show data regarding forcings for $H_{\text{amp}} = 10, 50$, because no arrangement takes place. Most likely the energy landscape is too trivial.

⁹ Because $P_{H_{\text{amp}}, L}(A_F, n)$ is not defined over all the samples (it is hard to reach many different valleys and it may not happen in all the simulations), the errors on $P_{H_{\text{amp}}, L}(A_F, n)$ were calculated by resampling over the reduced data sets with the bootstrap method.

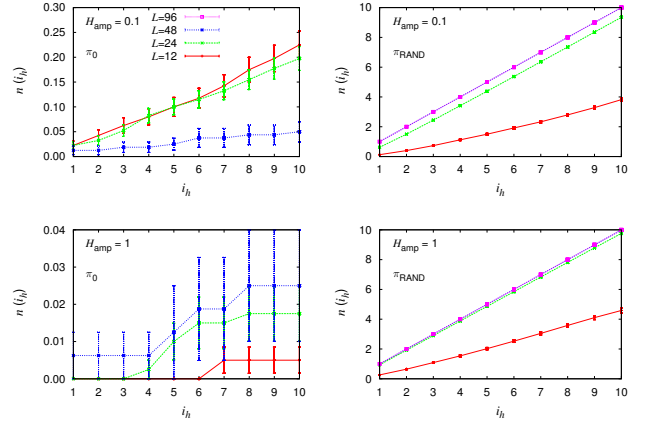


Figure 13. Average number of rearrangements $n(i_h)$ for forcings along $|\vec{\pi}_0\rangle$ (left) and along $|\vec{\pi}_{\text{RAND}}\rangle$ (right). The data come from $H_{\text{amp}} = 0.1$ (top) and $H_{\text{amp}} = 1$ (bottom). When the lattice becomes large enough, the forcings along $|\vec{\pi}_{\text{RAND}}\rangle$ lead to a new IS every time i_h is increased. The data from the $|\vec{\pi}_0\rangle$ and $H_{\text{amp}} = 1$ can be said to be in the regime of first rearrangement.

the barrier. Still, it may happen that the IS obtained with the Hamiltonian \mathcal{H}_F have an energy lower than the energy $E_{\text{RF}}(|s^{(\text{IS})}\rangle)$ calculated with \mathcal{H}_{RF} , so in a strict sense ΔE is not positive definite. To overcome this issue, we measure the barrier ΔE^* from the arriving IS instead of the starting one, that has the advantage of being positive definite. We see in figure 14 that while the energy barriers from random forcings increase with the system size (the growth is $O(N)$), while those within the TLS (along the softest mode) do not grow at all.

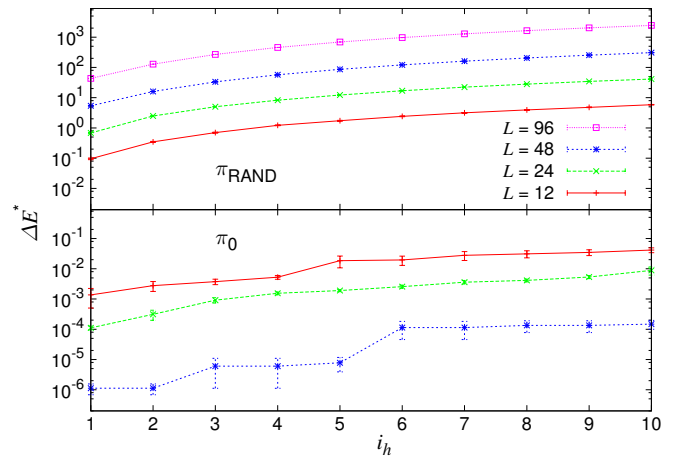


Figure 14. Average energy barrier ΔE^* for forcings along $|\vec{\pi}_{\text{RAND}}\rangle$ (top) and $|\vec{\pi}_0\rangle$ (bottom), for random fields of amplitude $H_{\text{amp}} = 0.1$ (data for $|\vec{\pi}_0\rangle$ and $L = 96$ were not computed, see table I).

-
- [1] W. A. Phillips. *Amorphous Solids: Low-Temperature Properties*. Topics in Current Physics 24. Springer-Verlag Berlin Heidelberg, 1981.
- [2] U. Buchenau, N. Nücker, and A. J. Dianoux. Neutron scattering study of the low-frequency vibrations in vitreous silica. *Phys. Rev. Lett.*, 53:2316–2319, Dec 1984.
- [3] V.K. Malinovsky, V.N. Novikov, and A.P. Sokolov. Log-normal spectrum of low-energy vibrational excitations in glasses. *Physics Letters A*, 153(1):63 – 66, 1991.
- [4] V. Gurarie and J. T. Chalker. Bosonic excitations in random media. *Phys. Rev. B*, 68:134207, Oct 2003.
- [5] V. L. Gurevich, D. A. Parshin, and H. R. Schober. Anharmonicity, vibrational instability, and the boson peak in glasses. *Phys. Rev. B*, 67:094203, Mar 2003.
- [6] HGE Hentschel, Smarajit Karmakar, Edan Lerner, and Itamar Procaccia. Do athermal amorphous solids exist? *Physical Review E*, 83(6):061101, 2011.
- [7] Jie Lin and Matthieu Wyart. Mean-field description of plasticity in disordered solids. 2015.
- [8] A.J. Liu Ning Xu, D. M. Sussman and S. R. Nagel. Density of states for normal modes near instabilities in glasses modeled by jammed packings. in preparation, 2015.
- [9] M Wyart, SR Nagel, and TA Witten. Geometric origin of excess low-frequency vibrational modes in weakly connected amorphous solids. *EPL (Europhysics Letters)*, 72(3):486, 2005.
- [10] Matthieu Wyart. Marginal stability constrains force and pair distributions at random close packing. *Phys. Rev. Lett.*, 109:125502, Sep 2012.
- [11] Corey S. O’Hern, Leonardo E. Silbert, Andrea J. Liu, and Sidney R. Nagel. Jamming at zero temperature and zero applied stress: The epitome of disorder. *Phys. Rev. E*, 68:011306, Jul 2003.
- [12] S. Franz, G. Parisi, P. Urbani, and F. Zamponi. The simplest model of jamming. 2015.
- [13] S. Franz, G. Parisi, P. Urbani, and F. Zamponi. Universal spectrum of normal modes in low-temperature glasses: an exact solution. Submitted to PNAS, 2015.
- [14] M. Mézard, G. Parisi, N. Sourlas, G. Toulouse, and M.A. Virasoro. Nature of the spin-glass phase. *Phys. Rev. Lett.*, 52:1156, 1984.
- [15] P. Charbonneau, J. Kurchan, G. Parisi, P. Urbani, and F. Zamponi. Fractal free energy landscapes in structural glasses. *Nature Communications*, 5:3725, 2014.
- [16] M. Mézard, G. Parisi, and M. Virasoro. *Spin-Glass Theory and Beyond*. World Scientific, Singapore, 1987.
- [17] C. Lupo, G. Parisi, and F. Ricci-Tersenghi. 2015.
- [18] F Barahona. On the computational complexity of ising spin glass models. *Journal of Physics A: Mathematical and General*, 15(10):3241, 1982.
- [19] P.W. Anderson. Localisation theory and cumn problems - spin glasses. *Materials Research Bulletin*, 5:549, 1970.
- [20] A J Bray and M A Moore. Metastable states, internal field distributions and magnetic excitations in spin glasses. *Journal of Physics C: Solid State Physics*, 14(19):2629, 1981.
- [21] T S Grigera, V Martin-Mayor, G Parisi, P Urbani, and P Verrocchio. On the high-density expansion for euclidean random matrices. *Journal of Statistical Mechanics: Theory and Experiment*, 2011(02):P02015, 2011.
- [22] Matthieu Wyart, Leonardo E. Silbert, Sidney R. Nagel, and Thomas A. Witten. Effects of compression on the vibrational modes of marginally jammed solids. *Phys. Rev. E*, 72:051306, Nov 2005.
- [23] Edan Lerner, Gustavo During, and Matthieu Wyart. Low-energy non-linear excitations in sphere packings. *Soft Matter*, 9:8252–8263, 2013.
- [24] Eric DeGiuli, Adrien Laversanne-Finot, Gustavo During, Edan Lerner, and Matthieu Wyart. Effects of coordination and pressure on sound attenuation, boson peak and elasticity in amorphous solids. *Soft Matter*, 10:5628–5644, 2014.
- [25] E. DeGiuli, E. Lerner, and M. Wyart. Theory of the jamming transition at finite temperature. *The Journal of Chemical Physics*, 142(16):–, 2015.
- [26] Auditya Sharma and A. P. Young. de almeida’s line in vector spin glasses. *Phys. Rev. E*, 81:061115, Jun 2010.
- [27] W. Kob, S. Roldán-Vargas, and L. Berthier. Non-monotonic temperature evolution of dynamic correlations in glass-forming liquids. *Nature Physics*, 8:164, 2012.
- [28] Chiara Cammarota and Giulio Biroli. Random pinning glass transition: Hallmarks, mean-field theory and renormalization group analysis. *J. Chem. Phys.*, 138(12):–, 2013.
- [29] Carolina Brito, Giorgio Parisi, and Francesco Zamponi. Jamming transition of randomly pinned systems. *Soft Matter*, 9(35):8540–8546, 2013.
- [30] Shreyas Gokhale, K. Hima Nagamanasa, Rajesh Ganapathy, and A. K. Sood. Growing dynamical facilitation on approaching the random pinning colloidal glass transition. *Nat Commun*, 5:4685, 2014.
- [31] K. Hima Nagamanasa, Shreyas Gokhale, A. K. Sood, and Rajesh Ganapathy. Direct measurements of growing amorphous order and non-monotonic dynamic correlations in a colloidal glass-former. *Nat Phys*, 11:403–408, 2015.
- [32] R B Grzonka and M A Moore. Computer studies of two-level systems of the three-dimensional planar spin glass. *Journal of Physics C: Solid State Physics*, 17(15):2785, 1984.
- [33] M. Baity-Jesi, V. Martín-Mayor, G. Parisi, and S. Pérez-Gaviro. In preparation, 2016.
- [34] K. Huang. *Statistical Mechanics*. John Wiley and Sons, Hoboken, NJ, second edition, 1987.
- [35] T.S. Chihara. *An Introduction to Orthogonal Polynomials*. Gordon & Breach, New York, 1978.
- [36] P Turchi, F Ducastelle, and G Treglia. Band gaps and asymptotic behaviour of continued fraction coefficients. *Journal of Physics C: Solid State Physics*, 15(13):2891, 1982.
- [37] J. L. Alonso, L. A. Fernández, F. Guinea, V. Laliena, and V. Martín-Mayor. Variational mean-field approach to the double-exchange model. *Phys. Rev. B*, 63:054411, Jan 2001.
- [38] D.C. Sorensen, R.B. Lehoucq, C. Yang, and K. Maschhoff, 1996-2008. Arpack, ARnoldi PACKage, www.caam.rice.edu/software/ARPACK/.
- [39] N. Xu, V. Vitelli, A. J. Liu, and S. R. Nagel. Anharmonic and quasi-localized vibrations in jammed solids—modes for mechanical failure. *Europhys. Lett.*, 90(5):56001, 2010.
- [40] Eric DeGiuli, Edan Lerner, Carolina Brito, and Matthieu Wyart. Force distribution affects vibrational prop-

- erties in hard-sphere glasses. *Proc. Nat. Ac. Sci.*, 111(48):17054–17059, 2014.
- [41] Patrick Charbonneau, Eric I. Corwin, Giorgio Parisi, and Francesco Zamponi. Jamming criticality revealed by removing localized buckling excitations. *Phys. Rev. Lett.*, 114:125504, Mar 2015.
- [42] P. W. Anderson, B. I. Halperin, and C. M. Varma. Anomalous low-temperature thermal properties of glasses and spin glasses. *Phil. Mag.*, 25(1):1–9, 1972.
- [43] W.A. Phillips. Tunneling states in amorphous solids. *J. Low Temp. Phys.*, 7(3-4):351–360, 1972.
- [44] W A Phillips. Two-level states in glasses. *Rep. Prog. Phys.*, 50(12):1657, 1987.
- [45] J. Lisenfeld, G.J. Grabovskij, C. Müller, J.H. Cole, G. Weiss, and A.V. Ustinov. Observation of directly interacting coherent two-level systems in an amorphous material. *Nat. Comm.*, 6:6182, 2015.
- [46] T. Pérez-Castañeda, R. J. Jiménez-Riobóo, and M. A. Ramos. Do Two-Level Systems and Boson Peak persist or vanish in hyperaged geological glasses of amber? *Phil. Mag.*, 2015. In press.
- [47] M. Baity-Jesi. Energy landscape in three-dimensional heisenberg spin glasses. Master’s thesis, Sapienza, Università di Roma, Rome, Italy, January 2011.
- [48] M. Baity-Jesi and G. Parisi. Inherent structures in m-component spin glasses. *Phys. Rev. B*, 91(13):134203, April 2015.
- [49] D. J. Amit and V. Martin-Mayor. *Field Theory, the Renormalization Group and Critical Phenomena*. World Scientific, Singapore, third edition, 2005.
- [50] L. A. Fernandez, V. Martin-Mayor, S. Perez-Gaviro, A. Tarancon, and A. P. Young. Phase transition in the three dimensional Heisenberg spin glass: Finite-size scaling analysis. *Phys. Rev. B*, 80:024422, 2009.
- [51] M. Gell-Mann and M. Lévy. The axial vector current in beta decay. *Il Nuovo Cimento*, 16(4):705–726, 1960.